Available online at www.sciencedirect.com
ScienceDirect
Journal of Sound and Vibration 312 (2008) 526–550
JOURNAL OF SOUND AND VIBRATION
www.elsevier.com/locate/jsvi

Shape optimization of multi-chamber cross-flow mufflers by SA optimization

Min-Chie Chiu[a,*], Ying-Chun Chang[b]

[a]Department of Automatic Control Engineering, Chungchou Institute of Technology, 6, Lane 2, Section 3, Shanchiao Road, Yuanlin, Changhua 51003, Taiwan, ROC
[b]Department of Mechanical Engineering, Tatung University, Taipei, Taiwan, ROC

Received 1 June 2007; received in revised form 31 October 2007; accepted 3 November 2007
Available online 20 February 2008

Abstract

It is essential when searching for an efficient acoustical mechanism to have an optimally shaped muffler designed specially for the constrained space found in today's plants. Because the research work of optimally shaped straight silencers in conjunction with multi-chamber cross-flow perforated ducts is rarely addressed, this paper will not only analyze the sound transmission loss (STL) of three kinds of cross-flow perforated mufflers but also will analyze the optimal design shape within a limited space.

In this paper, the four-pole system matrix used in evaluating acoustic performance is derived by using the decoupled numerical method. Moreover, a simulated annealing (SA) algorithm, a robust scheme in searching for the global optimum by imitating the softening process of metal, has been adopted during shape optimization. To reassure SA's correctness, the STL's maximization of three kinds of muffles with respect to one-tone and dual-tone noise is exemplified. Furthermore, the optimization of mufflers with respect to an octave-band fan noise by the simulated algorithm has been introduced and fully discussed. Before the SA operation can be carried out, an accuracy check of the mathematical model with respect to cross-flow perforated mufflers has to be performed by Munjal's analytical data and experimental data.

The optimal result in eliminating broadband noise reveals that the cross-flow perforated muffler with more chambers is far superior at noise reduction than a muffler with fewer chambers. Consequently, the approach used for the optimal design of noise elimination proposed in this study is certainly easy and efficient.

1. Introduction

The research of mufflers was started by Davis et al. [1]. To increase a muffler's acoustical performance, the assessment of a new acoustical element—cross-flow mechanism with double internal perforated tubes—was proposed and investigated by Munjal et al. [2]. On the basis of the coupled differential equations, a series of theories and numerical techniques in decoupling the acoustical problems have been widely proposed [3–7]. Considering the flowing effect, Munjal [8] and Peat [9] publicized the generalized decoupling and numerical decoupling methods, which supercede the drawbacks in previous studies. Because the constrained problem is

*Corresponding author.
E-mail address: minchie.chiu@msa.hinet.net (M.-C. Chiu).

0022-460X/$ - see front matter © 2007 Elsevier Ltd. All rights reserved.
doi:10.1016/j.jsv.2007.11.003

Nomenclature

c_o	sound speed ($\mathrm{m\,s^{-1}}$)
dh_i	the diameter of perforated hole on ith inner tube (m)
D_i, D_{i+1}	diameter of the inner perforated tubes inside the ith chamber (m)
D_o	diameter of the outer tube (m)
f	cyclic frequency (Hz)
H	dynamic head (Pa)
$\mathrm{iter}_{\max}$	maximum iteration
j	imaginary unit
k	wave number ($=\omega/c_o$)
kk	cooling rate in SA
L_1, L_2	lengths of inlet/outlet straight ducts (m)
L_{Ai}, L_{Bi}	length of the un-perforated segments within the ith chamber (m)
L_{Ci}	length of the perforated segment within the ith chamber (m)
L_0	total length of the muffler (m)
L_{Zi}	length of the ith cross-flow chamber ($=L_{Ai}+L_{Ci}+L_{Bi}$) (m)
M	mean flow Mach number
OBJ_i	objective function (dB)
$\bar{p}_i$	acoustic pressure at ith node (Pa)
$\mathrm{pb}(T)$	transition probability
Q	volume flow rate of venting gas ($\mathrm{m^3\,s^{-1}}$)
S_i	section area at ith node ($\mathrm{m^2}$)
STL	sound transmission loss (dB)
SWLO	unsilenced sound power level inside the muffler's inlet (dB)
SWL_T	overall sound power level inside the muffler's output (dB)
t_i	the thickness of the ith inner perforated tube (m)
$\mathrm{TS1}_{ij}$, $\mathrm{TS2}_{ij}$	components of four-pole transfer matrices for straight ducts
TPCF_{ij}	components of a four-pole transfer matrix for a cross-flow perforated duct
T^*_{ij}	components of a four-pole transfer system matrix
$\bar{u}_i$	acoustic particle velocity at ith node ($\mathrm{m\,s^{-1}}$)
V_i	mean flow velocity at ith node ($\mathrm{m\,s^{-1}}$)
x	open area ratio
ρ_o	air density ($\mathrm{kg\,m^{-3}}$)
η_i	the porosity of the ith inner perforated tube
Δp	mean pressure drop (Pa)

mostly concerned with the necessity of operation and maintenance in practical engineering work, there is a growing need to optimize the acoustical performance under a fixed space. Yet, the need to investigate the optimal muffler design under space constraints is rarely tackled.

In previous papers, the shape optimizations of straight simple-expansion mufflers have been discussed [10–12]. In order to improve the performance of the noise control device, the cross-flow perforated mufflers with multi-chambers that were arrived at by using the novel scheme of simulated annealing (SA) is presented. In this paper, the numerical decoupling methods in conjunction with the SA to minimize the overall value of SWL by adjusting the shape, the perforated ratio, and the hole's diameter of the muffler under space constraints are used.

2. Theorretical background

In this paper, one-, two-, and three-chamber cross-flow perforated mufflers were adopted for the noise elimination in the fan room shown in Fig. 1. The outlines, acoustic pressure $\bar{p}$ and acoustic particle velocity $\bar{u}$, of these mufflers are shown in Figs. 2–4.

2.1. A one-chamber cross-flow perforated muffler

As indicated in Fig. 2, individual transfer matrixes with respect to each case of straight ducts and cross-flow perforated tubes are described as follows [8–12]:

$$\begin{pmatrix} \bar{p}_1 \\ \rho_o c_o \bar{u}_1 \end{pmatrix} = \mathrm{e}^{-\mathrm{j}M_1 k(L_1+L_{A1})/(1-M_1^2)} \begin{bmatrix} \mathrm{TS1}_{1,1} & \mathrm{TS1}_{1,2} \\ \mathrm{TS1}_{2,1} & \mathrm{TS1}_{2,2} \end{bmatrix} \begin{pmatrix} \bar{p}_2 \\ \rho_o c_o \bar{u}_2 \end{pmatrix}, \tag{1a}$$

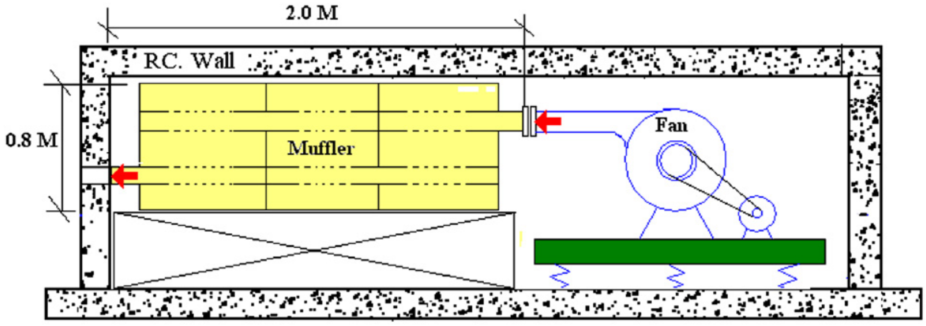

Fig. 1. Noise elimination of a fan noise inside a limited space.

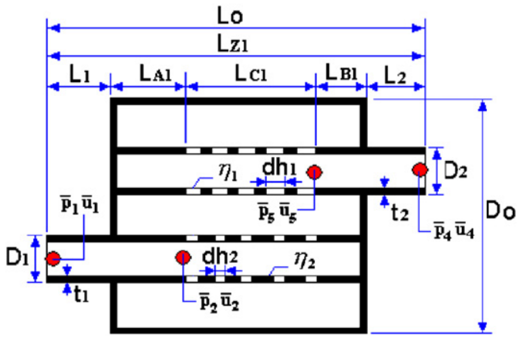

Fig. 2. The outline of a one-chamber cross-flow perforated muffler.

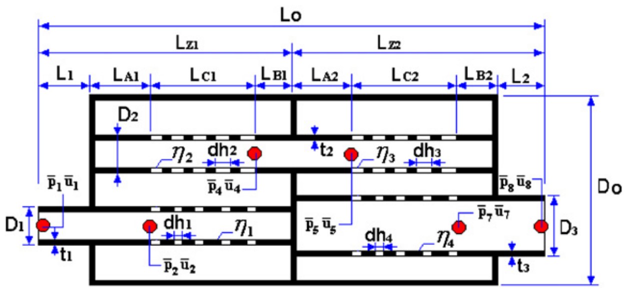

Fig. 3. The outline of a two-chamber cross-flow perforated muffler.

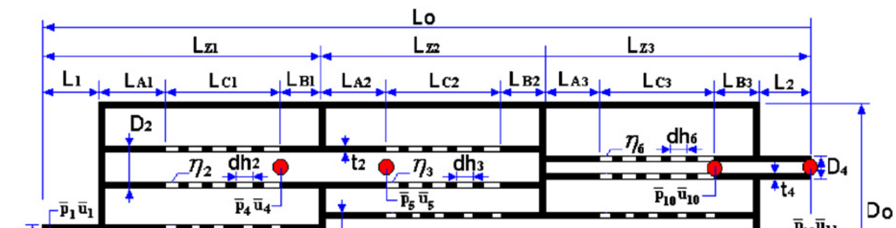

Fig. 4. The outline of a three-chamber cross-flow perforated muffler.

$$\mathrm{TS1}_{1,1} = \cos\left[\frac{k(L_1 + L_{A1})}{1 - M_1^2}\right], \quad \mathrm{TS1}_{1,2} = \mathrm{j}\ \sin\left[\frac{k(L_1 + L_{A1})}{1 - M_1^2}\right],$$
$$\mathrm{TS1}_{2,1} = \mathrm{j}\ \sin\left[\frac{k(L_1 + L_{A1})}{1 - M_1^2}\right], \quad \mathrm{TS1}_{2,2} = \cos\left[\frac{k(L_1 + L_{A1})}{1 - M_1^2}\right], \tag{1b}$$

$$\begin{pmatrix} \bar{p}_2 \\ \rho_o c_o \bar{u}_2 \end{pmatrix} = \begin{bmatrix} \mathrm{TPCF1}_{1,1} & \mathrm{TPCF1}_{1,2} \\ \mathrm{TPCF1}_{2,1} & \mathrm{TPCF1}_{2,2} \end{bmatrix} \begin{pmatrix} \bar{p}_4 \\ \rho_o c_o \bar{u}_4 \end{pmatrix}, \tag{2}$$

$$\begin{pmatrix} \bar{p}_4 \\ \rho_o c_o \bar{u}_4 \end{pmatrix} = \mathrm{e}^{-\mathrm{j}M_4 k(L_2 + L_{B1})/(1-M_4^2)} \begin{bmatrix} \mathrm{TS2}_{1,1} & \mathrm{TS2}_{1,2} \\ \mathrm{TS2}_{2,1} & \mathrm{TS2}_{2,2} \end{bmatrix} \begin{pmatrix} \bar{p}_5 \\ \rho_o c_o \bar{u}_5 \end{pmatrix}, \tag{3a}$$

$$\mathrm{TS2}_{1,1} = \cos\left[\frac{k(L_2 + L_{B1})}{1 - M_4^2}\right], \quad \mathrm{TS2}_{1,2} = \mathrm{j}\ \sin\left[\frac{k(L_2 + L_{B1})}{1 - M_4^2}\right],$$
$$\mathrm{TS2}_{2,1} = \mathrm{j}\ \sin\left[\frac{k(L_2 + L_{B1})}{1 - M_4^2}\right], \quad \mathrm{TS2}_{2,2} = \cos\left[\frac{k(L_2 + L_{B1})}{1 - M_4^2}\right]. \tag{3b}$$

The total transfer matrix assembled by multiplication is

$$\begin{pmatrix} \bar{p}_1 \\ \rho_o c_o \bar{u}_1 \end{pmatrix} = \mathrm{e}^{-\mathrm{j}k[(M_1(L_1+L_{A1})/1-M_1^2)+(M_1(L_2+L_{B1})/1-M_4^2)]} \begin{bmatrix} \mathrm{TS1}_{1,1} & \mathrm{TS1}_{1,2} \\ \mathrm{TS1}_{2,1} & \mathrm{TS1}_{2,2} \end{bmatrix}$$
$$\times \begin{bmatrix} \mathrm{TPCF1}_{1,1} & \mathrm{TPCF1}_{1,2} \\ \mathrm{TPCF1}_{2,1} & \mathrm{TPCF1}_{2,2} \end{bmatrix} \begin{bmatrix} \mathrm{TS2}_{1,1} & \mathrm{TS2}_{1,2} \\ \mathrm{TS2}_{2,1} & \mathrm{TS2}_{2,2} \end{bmatrix} \begin{pmatrix} \bar{p}_5 \\ \rho_o c_o \bar{u}_5 \end{pmatrix}. \tag{4a}$$

A simplified form in the matrix is expressed as

$$\begin{pmatrix} \bar{p}_1 \\ \rho_o c_o \bar{u}_1 \end{pmatrix} = \begin{bmatrix} T_{11}^* & T_{12}^* \\ T_{21}^* & T_{22}^* \end{bmatrix} \begin{pmatrix} \bar{p}_5 \\ \rho_o c_o \bar{u}_5 \end{pmatrix}. \tag{4b}$$

Under the assumption of the fixed thickness of the tubes ($t_1 = t_2 = 0.001$) and the symmetric design ($L_{A1} = L_{B1}$; $L_1 = L_2$), the sound transmission loss (STL) of a muffler is defined as [8]

$$\mathrm{STL}(Q, f, \mathrm{Aff}_1, \mathrm{Aff}_2, D_1, D_2, \mathrm{dh}_1, \eta_1, \mathrm{dh}_2, \eta_2) = 20\ \log\left(\frac{|T_{11}^* + T_{12}^* + T_{21}^* + T_{22}^*|}{2}\right) + 10\ \log\left(\frac{S_1}{S_5}\right), \tag{5a}$$

where

$$\mathrm{Aff}_1 = L_{Z1}/L_0, \quad \mathrm{Aff}_2 = L_{C1}/L_0, \quad L_{Z1} = L_{A1} + L_{B1} + L_{C1},$$
$$L_{A1} = L_{B1} = (L_{Z1} - L_{C1})/2, \quad L_1 = L_2 = (L_0 - L_{Z1})/2. \tag{5b}$$

The mean pressure drop (Δp) of a one-chamber cross-flow muffler investigated by Munjal et al. [13] is

$$\Delta p = \mathrm{Max}\{H_1(4.2\mathrm{e}^{-0.06x1} + 16.7\mathrm{e}^{-2.03x1}), H_2(4.2\mathrm{e}^{-0.06x2} + 16.7\mathrm{e}^{-2.03x2})\}, \tag{6a}$$

$$H_1 = \rho V_1^2/2, \quad H_2 = \rho V_2^2/2, \quad x_1 = 4L_{C1}\eta_1/D_1, \quad x_2 = 4L_{C1}\eta_2/D_2. \tag{6b}$$

2.2. A two-chamber cross-flow perforated muffler

As indicated in Fig. 3, individual transfer matrixes with respect to each case of straight ducts and cross-flow perforated ducts are described as follows [8–12]:

$$\begin{pmatrix} \bar{p}_1 \\ \rho_o c_o \bar{u}_1 \end{pmatrix} = \mathrm{e}^{-\mathrm{j}M_1 k(L_1 + L_{A1})/(1-M_1^2)} \begin{bmatrix} \mathrm{TS1}_{1,1} & \mathrm{TS1}_{1,2} \\ \mathrm{TS1}_{2,1} & \mathrm{TS1}_{2,2} \end{bmatrix} \begin{pmatrix} \bar{p}_2 \\ \rho_o c_o \bar{u}_2 \end{pmatrix}, \tag{7a}$$

$$\mathrm{TS1}_{1,1}=\cos\left[\frac{k(L_1+L_{A1})}{1-M_1^2}\right],\quad \mathrm{TS1}_{1,2}=\mathrm{j}\,\sin\left[\frac{k(L_1+L_{A1})}{1-M_1^2}\right],$$
$$\mathrm{TS1}_{2,1}=\mathrm{j}\,\sin\left[\frac{k(L_1+L_{A1})}{1-M_1^2}\right],\quad \mathrm{TS1}_{2,2}=\cos\left[\frac{k(L_1+L_{A1})}{1-M_1^2}\right], \tag{7b}$$

$$\begin{pmatrix}\bar{p}_2\\ \rho_o c_o \bar{u}_2\end{pmatrix}=\begin{bmatrix}\mathrm{TPCF1}_{1,1} & \mathrm{TPCF1}_{1,2}\\ \mathrm{TPCF1}_{2,1} & \mathrm{TPCF1}_{2,2}\end{bmatrix}\begin{pmatrix}\bar{p}_4\\ \rho_o c_o \bar{u}_4\end{pmatrix}, \tag{8}$$

$$\begin{pmatrix}\bar{p}_5\\ \rho_o c_o \bar{u}_5\end{pmatrix}=\begin{bmatrix}\mathrm{TPCF2}_{1,1} & \mathrm{TPCF2}_{1,2}\\ \mathrm{TPCF2}_{2,1} & \mathrm{TPCF2}_{2,2}\end{bmatrix}\begin{pmatrix}\bar{p}_7\\ \rho_o c_o \bar{u}_7\end{pmatrix}, \tag{9}$$

$$\begin{pmatrix}\bar{p}_7\\ \rho_o c_o \bar{u}_7\end{pmatrix}=\mathrm{e}^{-\mathrm{j}M_7k(L_2+L_{B2})/(1-M_7^2)}\begin{bmatrix}\mathrm{TS2}_{1,1} & \mathrm{TS2}_{1,2}\\ \mathrm{TS2}_{2,1} & \mathrm{TS2}_{2,2}\end{bmatrix}\begin{pmatrix}\bar{p}_8\\ \rho_o c_o \bar{u}_8\end{pmatrix}, \tag{10a}$$

$$\mathrm{TS2}_{1,1}=\cos\left[\frac{k(L_2+L_{B2})}{1-M_7^2}\right],\quad \mathrm{TS2}_{1,2}=\mathrm{j}\,\sin\left[\frac{k(L_2+L_{B2})}{1-M_7^2}\right],$$
$$\mathrm{TS2}_{2,1}=\mathrm{j}\,\sin\left[\frac{k(L_2+L_{B2})}{1-M_7^2}\right],\quad \mathrm{TS2}_{2,2}=\cos\left[\frac{k(L_2+L_{B2})}{1-M_7^2}\right]. \tag{10b}$$

The total transfer matrix assembled by multiplication is

$$\begin{pmatrix}\bar{p}_1\\ \rho_o c_o \bar{u}_1\end{pmatrix}=\mathrm{e}^{-\mathrm{j}k[(M_1(L_1+L_{A1})/1-M_1^2)+(M_7(L_2+L_{B2})/1-M_7^2)]}\begin{bmatrix}\mathrm{TS1}_{1,1} & \mathrm{TS1}_{1,2}\\ \mathrm{TS1}_{2,1} & \mathrm{TS1}_{2,2}\end{bmatrix}\begin{bmatrix}\mathrm{TPCF1}_{1,1} & \mathrm{TPCF1}_{1,2}\\ \mathrm{TPCF1}_{2,1} & \mathrm{TPCF1}_{2,2}\end{bmatrix}$$
$$\times\begin{bmatrix}\mathrm{TPCF2}_{1,1} & \mathrm{TPCF2}_{1,2}\\ \mathrm{TPCF2}_{2,1} & \mathrm{TPCF2}_{2,2}\end{bmatrix}\begin{bmatrix}\mathrm{TS2}_{1,1} & \mathrm{TS2}_{1,2}\\ \mathrm{TS2}_{2,1} & \mathrm{TS2}_{2,2}\end{bmatrix}\begin{pmatrix}\bar{p}_8\\ \rho_o c_o \bar{u}_8\end{pmatrix}. \tag{11a}$$

A simplified form in the matrix is expressed as

$$\begin{pmatrix}\bar{p}_1\\ \rho_o c_o \bar{u}_1\end{pmatrix}=\begin{bmatrix}T_{11}^* & T_{12}^*\\ T_{21}^* & T_{22}^*\end{bmatrix}\begin{pmatrix}\bar{p}_8\\ \rho_o c_o \bar{u}_8\end{pmatrix}. \tag{11b}$$

Under the assumption of the fixed thickness of the tubes ($t_1=t_2=t_3=0.001$ m) and the symmetric design ($L_{A1}=L_{B1}$, $L_{A2}=L_{B2}$, $L_1=L_2$), the STL of a muffler is defined as [8]

$$\begin{aligned}&\mathrm{STL}(Q,f,\mathrm{Aff}_1,\mathrm{Aff}_2,\mathrm{Aff}_3,\mathrm{Aff}_4,D_1,D_2,D_3,\mathrm{dh}_1,\eta_1,\mathrm{dh}_2,\eta_2,\mathrm{dh}_3,\eta_3,\mathrm{dh}_4,\eta_4)\\ &\quad=20\log\left(\frac{|T_{11}^*+T_{12}^*+T_{21}^*+T_{22}^*|}{2}\right)+10\log\left(\frac{S_1}{S_7}\right),\end{aligned} \tag{12a}$$

where

$$\begin{aligned}&\mathrm{Aff}_1=L_{Z1}/L_0,\quad \mathrm{Aff}_2=L_{Z2}/L_0,\quad \mathrm{Aff}_3=L_{C1}/L_{Z1},\quad \mathrm{Aff}_4=L_{C2}/L_{Z2},\\ &L_{A1}=L_{B1}=(L_{Z1}-L_{C1})/2,\quad L_{A2}=L_{B2}=(L_{Z2}-L_{C2})/2,\quad L_1=L_2=(L_0-L_{Z1}-L_{Z2})/2.\end{aligned} \tag{12b}$$

Similarly, the mean pressure drop (Δp) of a two-chamber muffler can be expressed as [13]

$$\begin{aligned}\Delta p=&\,\mathrm{Max}\{H_1(4.2\mathrm{e}^{-0.06x1}+16.7\mathrm{e}^{-2.03x1}),H_2(4.2\mathrm{e}^{-0.06x2}+16.7\mathrm{e}^{-2.03x2})\}\\ &+\mathrm{Max}\{H_3(4.2\mathrm{e}^{-0.06x3}+16.7\mathrm{e}^{-2.03x3}),H_4(4.2\mathrm{e}^{-0.06x4}+16.7\mathrm{e}^{-2.03x4})\},\end{aligned} \tag{13a}$$

$$H_1 = \rho V_1^2/2, \quad H_2 = \rho V_2^2/2, \quad H_3 = \rho V_3^2/2, \quad H_4 = \rho V_4^2/2,$$
$$x_1 = 4L_{C1}\eta_1/D_1, \quad x_2 = 4L_{C1}\eta_2/D_2, \quad x_3 = 4L_{C2}\eta_3/D_2, \quad x_4 = 4L_{C2}\eta_4/D_3. \tag{13b}$$

2.3. A three-chamber cross-flow perforated muffler

As indicated in Fig. 4, individual transfer matrixes with respect to each case of straight ducts and cross-flow perforated ducts are described as follows [8–12]:

$$\begin{pmatrix} \bar{p}_1 \\ \rho_o c_o \bar{u}_1 \end{pmatrix} = e^{-jM_1 k(L_1+L_{A1})/(1-M_1^2)} \begin{bmatrix} \mathrm{TS1}_{1,1} & \mathrm{TS1}_{1,2} \\ \mathrm{TS1}_{2,1} & \mathrm{TS1}_{2,2} \end{bmatrix} \begin{pmatrix} \bar{p}_2 \\ \rho_o c_o \bar{u}_2 \end{pmatrix}, \tag{14a}$$

$$\mathrm{TS1}_{1,1} = \cos\left[\frac{k(L_1+L_{A1})}{1-M_1^2}\right], \quad \mathrm{TS1}_{1,2} = \mathrm{j}\sin\left[\frac{k(L_1+L_{A1})}{1-M_1^2}\right],$$
$$\mathrm{TS1}_{2,1} = \mathrm{j}\sin\left[\frac{k(L_1+L_{A1})}{1-M_1^2}\right], \quad \mathrm{TS1}_{2,2} = \cos\left[\frac{k(L_1+L_{A1})}{1-M_1^2}\right], \tag{14b}$$

$$\begin{pmatrix} \bar{p}_2 \\ \rho_o c_o \bar{u}_2 \end{pmatrix} = \begin{bmatrix} \mathrm{TPCF1}_{1,1} & \mathrm{TPCF1}_{1,2} \\ \mathrm{TPCF1}_{2,1} & \mathrm{TPCF1}_{2,2} \end{bmatrix} \begin{pmatrix} \bar{p}_4 \\ \rho_o c_o \bar{u}_4 \end{pmatrix}, \tag{15}$$

$$\begin{pmatrix} \bar{p}_5 \\ \rho_o c_o \bar{u}_5 \end{pmatrix} = \begin{bmatrix} \mathrm{TPCF2}_{1,1} & \mathrm{TPCF2}_{1,2} \\ \mathrm{TPCF2}_{2,1} & \mathrm{TPCF2}_{2,2} \end{bmatrix} \begin{pmatrix} \bar{p}_7 \\ \rho_o c_o \bar{u}_7 \end{pmatrix}, \tag{16}$$

$$\begin{pmatrix} \bar{p}_8 \\ \rho_o c_o \bar{u}_8 \end{pmatrix} = \begin{bmatrix} \mathrm{TPCF3}_{1,1} & \mathrm{TPCF3}_{1,2} \\ \mathrm{TPCF3}_{2,1} & \mathrm{TPCF3}_{2,2} \end{bmatrix} \begin{pmatrix} \bar{p}_{10} \\ \rho_o c_o \bar{u}_{10} \end{pmatrix}, \tag{17}$$

$$\begin{pmatrix} \bar{p}_{10} \\ \rho_o c_o \bar{u}_{10} \end{pmatrix} = e^{-jM_{10} k(L_2+L_{B3})/(1-M_{10}^2)} \begin{bmatrix} \mathrm{TS2}_{1,1} & \mathrm{TS2}_{1,2} \\ \mathrm{TS2}_{2,1} & \mathrm{TS2}_{2,2} \end{bmatrix} \begin{pmatrix} \bar{p}_{11} \\ \rho_o c_o \bar{u}_{11} \end{pmatrix}, \tag{18a}$$

$$\mathrm{TS2}_{1,1} = \cos\left[\frac{k(L_2+L_{B3})}{1-M_{10}^2}\right], \quad \mathrm{TS2}_{1,2} = \mathrm{j}\sin\left[\frac{k(L_2+L_{B3})}{1-M_{10}^2}\right],$$
$$\mathrm{TS2}_{2,1} = \mathrm{j}\sin\left[\frac{k(L_2+L_{B3})}{1-M_{10}^2}\right], \quad \mathrm{TS2}_{2,2} = \cos\left[\frac{k(L_2+L_{B3})}{1-M_{10}^2}\right]. \tag{18b}$$

The total transfer matrix assembled by multiplication is

$$\begin{pmatrix} \bar{p}_1 \\ \rho_o c_o \bar{u}_1 \end{pmatrix} = e^{-jk[(M_1(L_1+L_{A1})/1-M_1^2)+(M_{10}(L_2+L_{B3})/1-M_{10}^2)]} \begin{bmatrix} \mathrm{TS1}_{1,1} & \mathrm{TS1}_{1,2} \\ \mathrm{TS1}_{2,1} & \mathrm{TS1}_{2,2} \end{bmatrix} \begin{bmatrix} \mathrm{TPCF1}_{1,1} & \mathrm{TPCF1}_{1,2} \\ \mathrm{TPCF1}_{2,1} & \mathrm{TPCF1}_{2,2} \end{bmatrix}$$
$$\times \begin{bmatrix} \mathrm{TPCF2}_{1,1} & \mathrm{TPCF2}_{1,2} \\ \mathrm{TPCF2}_{2,1} & \mathrm{TPCF2}_{2,2} \end{bmatrix} \begin{bmatrix} \mathrm{TPCF3}_{1,1} & \mathrm{TPCF3}_{1,2} \\ \mathrm{TPFC3}_{2,1} & \mathrm{TPFC3}_{2,2} \end{bmatrix} \begin{bmatrix} \mathrm{TS2}_{1,1} & \mathrm{TS2}_{1,2} \\ \mathrm{TS2}_{2,1} & \mathrm{TS2}_{2,2} \end{bmatrix} \begin{pmatrix} \bar{p}_{11} \\ \rho_o c_o \bar{u}_{11} \end{pmatrix}. \tag{19a}$$

A simplified form in the matrix is expressed as

$$\begin{pmatrix} \bar{p}_1 \\ \rho_o c_o \bar{u}_1 \end{pmatrix} = \begin{bmatrix} T_{11}^* & T_{12}^* \\ T_{21}^* & T_{22}^* \end{bmatrix} \begin{pmatrix} \bar{p}_{11} \\ \rho_o c_o \bar{u}_{11} \end{pmatrix}. \tag{19b}$$

Under the assumption of the fixed thickness of the tubes ($t_1 = t_2 = t_3 = t_4 = 0.001$ m) and the symmetric design ($L_{A1} = L_{B1}$, $L_{A2} = L_{B2}$, $L_{A3} = L_{B3}$, $L_1 = L_2$), the STL of a muffler is defined as [8]

$$\begin{aligned}\mathrm{STL}&\begin{pmatrix} Q, f, \mathrm{Aff}_1, \mathrm{Aff}_2, \mathrm{Aff}_3, \mathrm{Aff}_4, \mathrm{Aff}_5, \mathrm{Aff}_6, D_1, D_2, D_3, D_4, \\ \mathrm{dh}_1, \eta_1, \mathrm{dh}_2, \eta_2, \mathrm{dh}_3, \eta_3, \mathrm{dh}_4, \eta_4, \mathrm{dh}_5, \eta_5, \mathrm{dh}_6, \eta_6 \end{pmatrix} \\ &= 20\log\left(\frac{|T_{11}^* + T_{12}^* + T_{21}^* + T_{22}^*|}{2}\right) + 10\log\left(\frac{S_1}{S_{10}}\right),\end{aligned} \tag{20a}$$

where

$$\begin{aligned}&\mathrm{Aff}_1 = L_{Z1}/L_0, \quad \mathrm{Aff}_2 = L_{Z2}/L_0, \quad \mathrm{Aff}_3 = L_{Z3}/L_0, \quad \mathrm{Aff}_4 = L_{C1}/L_{Z1}, \quad \mathrm{Aff}_5 = L_{C2}/L_{Z2}, \\ &\mathrm{Aff}_6 = L_{C3}/L_{Z3}, \quad L_{A1} = L_{B1} = (L_{Z1} - L_{C1})/2, \quad L_{A2} = L_{B2} = (L_{Z2} - L_{C2})/2, \\ &L_{A3} = L_{B3} = (L_{Z3} - L_{C3})/2, \quad L_1 = L_2 = (L_0 - L_{Z1} - L_{Z2})/2.\end{aligned} \tag{20b}$$

Equally, the mean pressure drop (Δp) of a two-chamber muffler can be expressed as [13]

$$\begin{aligned}\Delta p = &\,\mathrm{Max}\{H_1(4.2\mathrm{e}^{-0.06x1} + 16.7\mathrm{e}^{-2.03x1}), H_2(4.2\mathrm{e}^{-0.06x2} + 16.7\mathrm{e}^{-2.03x2})\} \\ &+ \mathrm{Max}\{H_3(4.2\mathrm{e}^{-0.06x3} + 16.7\mathrm{e}^{-2.03x3}), H_4(4.2\mathrm{e}^{-0.06x4} + 16.7\mathrm{e}^{-2.03x4})\} \\ &+ \mathrm{Max}\{H_5(4.2\mathrm{e}^{-0.06x5} + 16.7\mathrm{e}^{-2.03x5}) H_6(4.2\mathrm{e}^{-0.06x6} + 16.7\mathrm{e}^{-2.03x6})\},\end{aligned} \tag{21a}$$

$$\begin{aligned}&H_1 = \rho V_1^2/2, \quad H_2 = \rho V_2^2/2, \quad H_3 = \rho V_3^2/2, \quad H_4 = \rho V_4^2/2, \quad H_5 = \rho V_5^2/2, \\ &H_6 = \rho V_6^2/2, \quad x_1 = 4L_{C1}\eta_1/D_1, \quad x_2 = 4L_{C1}\eta_2/D_2, \quad x_3 = 4L_{C2}\eta_3/D_2, \\ &x_4 = 4L_{C2}\eta_4/D_3, \quad x_5 = 4L_{C3}\eta_5/D_3, \quad x_6 = 4L_{C3}\eta_6/D_4.\end{aligned} \tag{21b}$$

2.4. Overall sound power level

The silenced octave sound power level emitted from a silencer's outlet is

$$\mathrm{SWL}_i = \mathrm{SWLO}_i - \mathrm{STL}_i, \tag{22}$$

where

(1) SWLO_i is the original SWL at the inlet of a muffler (or pipe outlet), and i is the index of the octave band frequency;
(2) STL_i is the muffler's STL with respect to the relative octave band frequency;
(3) SWL_i is the silenced SWL at the outlet of a muffler with respect to the relative octave band frequency.

Finally, the overall SWL_T silenced by a muffler at the outlet is

$$\begin{aligned}\mathrm{SWL}_T &= 10\log\left\{\sum_{i=1}^{7} 10^{\mathrm{SWL}_i/10}\right\} \\ &= 10\log\left\{\begin{matrix} 10^{[\mathrm{SWLO}(f=63)-\mathrm{STL}(f=63)]/10} + 10^{[\mathrm{SWLO}(f=125)-\mathrm{STL}(f=125)]} + 10^{[\mathrm{SWLO}(f=250)-\mathrm{STL}(f=250)]/10} \\ +10^{[\mathrm{SWLO}(f=500)-\mathrm{STL}(f=500)]/10} + 10^{\mathrm{SWLO}(f=1000)-\mathrm{STL}(f=1000)]/10} \\ +10^{\mathrm{SWLO}(f=2000)-\mathrm{STL}(f=2000)]/10} + 10^{[\mathrm{SWLO}(f=4000)-\mathrm{STL}(f=4000)]/10} \end{matrix}\right\}.\end{aligned} \tag{23}$$

2.5. Objective function

By using the formula of Eqs. (5), (12), (20) and (23), the objective function used in SA optimization with respect to each type of muffler was established.

2.5.1. One-chamber cross-flow perforated muffler

(A) STL maximization for one-tone (f_1) noise:

$$\mathrm{OBJ}_{11} = \mathrm{STL}(Q, f_1, \mathrm{Aff}_1, \mathrm{Aff}_2, D_1, D_2, \mathrm{dh}_1, \eta_1, \mathrm{dh}_2, \eta_2). \tag{24}$$

(B) STL maximization for two-tone (f_2, f_3) noise:

$$\mathrm{STLA}_1 = \mathrm{STL}(Q, f_2, \mathrm{Aff}_1, \mathrm{Aff}_2, D_1, D_2, \mathrm{dh}_1, \eta_1, \mathrm{dh}_2, \eta_2), \tag{25a}$$

$$\mathrm{STLB}_1 = \mathrm{STL}(Q, f_3, \mathrm{Aff}_1, \mathrm{Aff}_2, D_1, D_2, \mathrm{dh}_1, \eta_1, \mathrm{dh}_2, \eta_2), \tag{25b}$$

$$\mathrm{OBJ}_{12} = \{\mathrm{STLA}_1 + \mathrm{STLB}_1\}/2. \tag{25c}$$

(C) SWL minimization for broadband noise:

To minimize the overall SWL, the objective function is

$$\mathrm{OBJ}_{13} = \mathrm{SWL}(Q, \mathrm{Aff}_1, \mathrm{Aff}_2, D_1, D_2, \mathrm{dh}_1, \eta_1, \mathrm{dh}_2, \eta_2). \tag{26}$$

The related ranges of parameters are:

$$\begin{gathered} f_1 = 150\ (\mathrm{Hz}), \quad f_2 = 100\ (\mathrm{Hz}), \quad f_3 = 200\ (\mathrm{Hz}), \quad Q = 0.03\ (\mathrm{m^3\,s^{-1}}); \quad D_o = 0.8\ (\mathrm{m}), \quad L_0 = 2.0\ (\mathrm{m}); \\ \mathrm{Aff}_1 : [0.2, 0.45]; \quad \mathrm{Aff}_2 : [0.3, 0.8]; \quad D_1 : [0.1, 0.35]; \quad D_2 : [0.1, 0.35]; \quad \mathrm{dh}_1 : [0.00175, 0.007]; \\ \eta_1 : [0.03, 0.1]; \quad \mathrm{dh}_2 : [0.00175, 0.007]; \quad \eta_2 : [0.03, 0.1]. \end{gathered} \tag{27}$$

2.5.2. Two-chamber cross-flow perforated muffler

(A) STL maximization for one-tone (f_1) noise:

$$\mathrm{OBJ}_{21} = \mathrm{STL}(Q, f_1, \mathrm{Aff}_1, \mathrm{Aff}_2, \mathrm{Aff}_3, \mathrm{Aff}_4, D_1, D_2, D_3, \mathrm{dh}_1, \eta_1, \mathrm{dh}_2, \eta_2, \mathrm{dh}_3, \eta_3, \mathrm{dh}_4, \eta_4). \tag{28}$$

(B) STL maximization for two-tone (f_2, f_3) noise:

$$\mathrm{STLA}_2 = \mathrm{STL}(Q, f_2, \mathrm{Aff}_1, \mathrm{Aff}_2, \mathrm{Aff}_3, \mathrm{Aff}_4, D_1, D_2, D_3, \mathrm{dh}_1, \eta_1, \mathrm{dh}_2, \eta_2, \mathrm{dh}_3, \eta_3, \mathrm{dh}_4, \eta_4), \tag{29a}$$

$$\mathrm{STLB}_2 = \mathrm{STL}(Q, f_3, \mathrm{Aff}_1, \mathrm{Aff}_2, \mathrm{Aff}_3, \mathrm{Aff}_4, D_1, D_2, D_3, \mathrm{dh}_1, \eta_1, \mathrm{dh}_2, \eta_2, \mathrm{dh}_3, \eta_3, \mathrm{dh}_4, \eta_4), \tag{29b}$$

$$\mathrm{OBJ}_{22} = \{\mathrm{STLA}_2 + \mathrm{STLB}_2\}/2. \tag{29c}$$

(C) SWL minimization for broadband noise:

To minimize the overall SWL, the objective function is

$$\mathrm{OBJ}_{23} = \mathrm{SWL}_T(Q, \mathrm{Aff}_1, \mathrm{Aff}_2, \mathrm{Aff}_3, \mathrm{Aff}_4, D_1, D_2, D_3, \mathrm{dh}_1, \eta_1, \mathrm{dh}_2, \eta_2, \mathrm{dh}_3, \eta_3, \mathrm{dh}_4, \eta_4). \tag{30}$$

3. Model check

Before performing the SA optimal simulation on the mufflers, an accuracy check of the mathematical models on a one-chamber cross-flow perforated muffler is performed using both of the analytical data from Munjal [2] and the experimental data in our work. As indicated in Figs. 5 and 6, the frequency characteristic between the theoretical data and Munjal's analytical data is different because of the shift in the fundamental resonance frequencies ($\sin(kL/(1-M^2))$ in which the flowing effect is considered. The performance curves are relatively accurate and in agreement. Therefore, the models of multi-chamber cross-flow and perforated mufflers in conjunction with the numerical searching method are applied to the shape optimization in the following section.

4. Case studies

In this paper, noise reduction with respect to a noisy induced fan (1200 rpm, 9 blades) installed inside a confined reinforced concrete (rc) room is exemplified and shown in Fig. 1. The sound power level (SWL) inside the fan's outlet is shown in Table 1 where the overall SWL reaches 138.9 dB. To realize the acoustical performances with respect to three kinds of mufflers (one-, two-, and three-chamber) installed at the fan's outlet, the numerical assessments linked to an optimizer will be performed. Before the minimization of a broadband noise is executed, the maximization of STL with respect to these mufflers at a targeted one tone (150 Hz) and two tones (100 and 200 Hz) will be carried out for the purpose of an accuracy verification on the SA method. As shown in Figs. 1–4, the available space for a muffler is 0.8 m in width, 0.8 m in height, and 2.0 m in length. The flow rate (Q) and thickness of a perforated tube (t) are preset as 0.03 ($m^3 s^{-1}$) and 0.001 (m), respectively; the corresponding OBJ functions, space constraints, and the ranges of design parameters for each muffler are summarized in Eqs. (24)–(30). Moreover, to assure the steady venting rate of

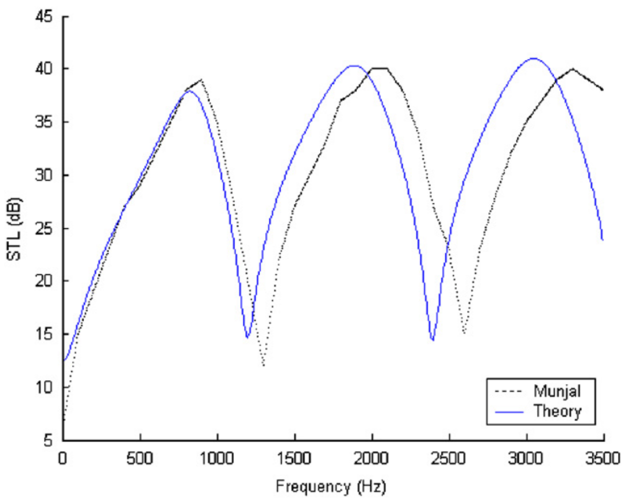

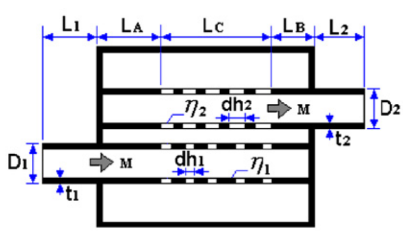

Fig. 5. Performance of a one-chamber cross-flow perforated muffler ($D_1 = 0.0493$ (m), $D_2 = 0.0493$ (m), $D_o = 0.1481$ (m), $L_A = L_B = 0.0064$, $L_c = 0.1286$ (m), $t_1 = t_2 = 0.0081$ (m), $dh_1 = dh_2 = 0.0035$ (m), $\eta_1 = \eta_2 = 0.039$, $M_1 = 0.1$) (analytical data are from Munjal et al. [2]).

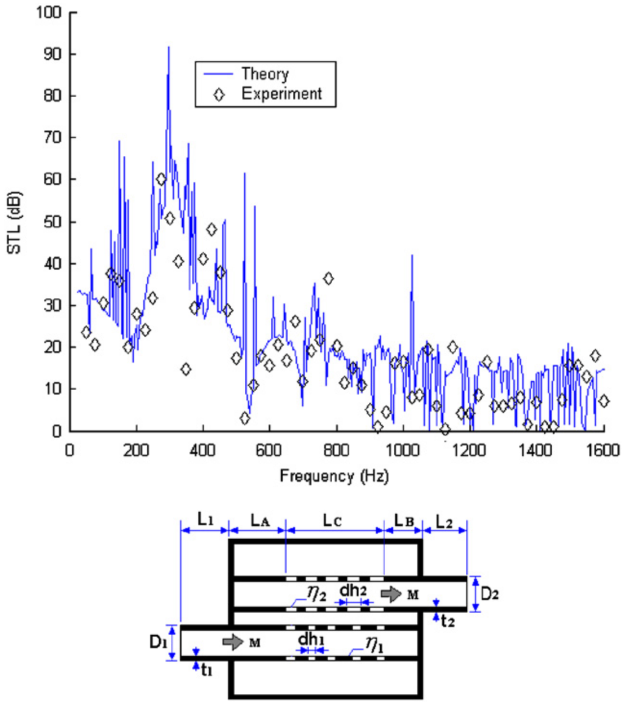

Fig. 6. Performance of a one-chamber cross-flow perforated muffler ($D_1 = 0.0254$ (m), $D_2 = 0.0254$ (m), $D_o = 0.254$ (m), $L_A = L_B = 0.2$, $L_c = 0.6$ (m), $t_1 = t_2 = 0.0081$ (m), $\mathrm{dh}_1 = \mathrm{dh}_2 = 0.003$ (m), $\eta_1 = \eta_2 = 0.06$, $M_1 = 0$).

Table 1
Unsilenced SWLs of a fan inside a duct outlet

Frequency (Hz)	125	250	500	1000	2000	4000
SWLO (dB)	138	128	125	125	120	120

the fan, the assumed allowable pressure drop (or back pressure) of a proposed muffler not exceeding 100 (Pa) is obligatory.

5. Simulated annealing algorithm

The SA algorithm is one kind of local search process which imitates the softening process (annealing) of metal. The basic concept behind SA was first introduced by Metropolis et al. [14] and developed by Kirkpatrick et al. [15]. From the viewpoint of the physical system, annealing is the process of heating and keeping a metal at a stabilized temperature when cooling it slowly. The slow cooling will allow the particles to keep their state close to the minimal energy state; therefore, the particles have a more homogeneous crystalline structure; if not, a fast cooling rate will result in a higher distortion energy stored inside the imperfect lattice.

A variation of the hill-climbing algorithm shown in Fig. 7 can be an analog to the SA's algorithm, The optimization process starts by generating a random initial solution. For a minimization process, all downhill movements for improvement are accepted for the decrement of the system's energy. Simultaneously, SA also allows movement resulting in solutions that are worse (uphill moves) than the current solution in order to escape from the local optimum.

As indicated in Fig. 8, to imitate the evolution of the SA algorithm, a new random solution (X') from the neighborhood of the current solution (X) is chosen and shown in Fig. 9. If the change in objective function (or energy) is negative (i.e. $\Delta F \leqslant 0$), the new solution will be acknowledged as the new current solution with

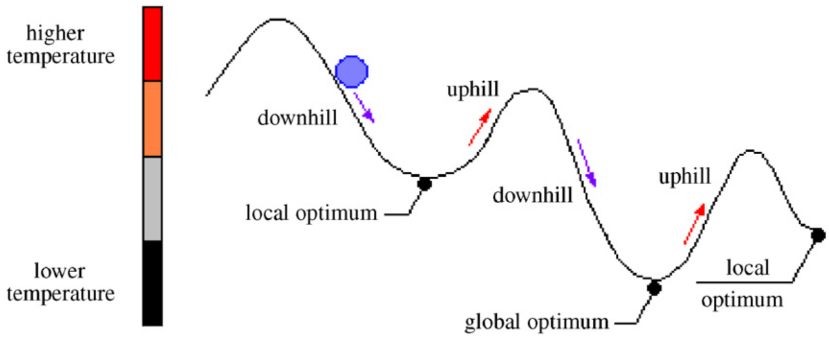

Fig. 7. SA algorithm from a physical viewpoint.

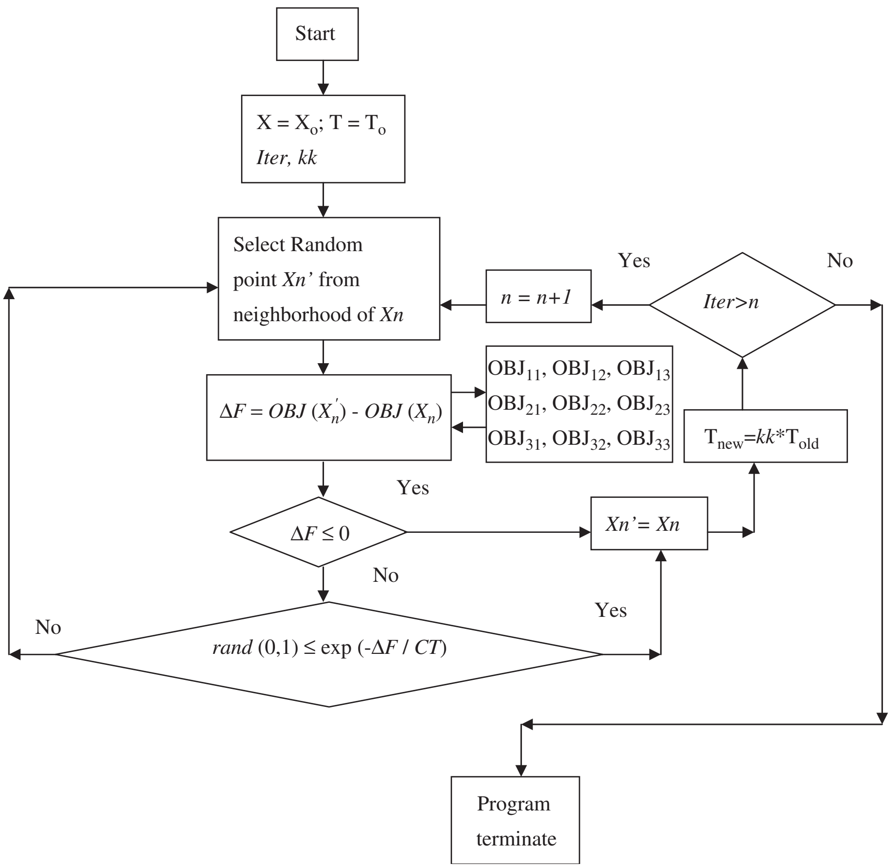

Fig. 8. Flow diagram of a SA optimization.

transition property ($\mathrm{pb}(X')$ of 1); if not (i.e. $\Delta F > 0$), the new transition property ($\mathrm{pb}(X')$) varied from 0 to 1 will be first calculated by the Boltzmann's factor ($\mathrm{pb}(X') = \exp(\Delta F/CT)$) as shown in Eq. (31):

$$\mathrm{pb}(X') = \begin{pmatrix} 1, & \Delta F \leqslant 0, \\ \exp\left(\dfrac{-\Delta F}{CT}\right), & \Delta F > 0, \end{pmatrix} \tag{31a}$$

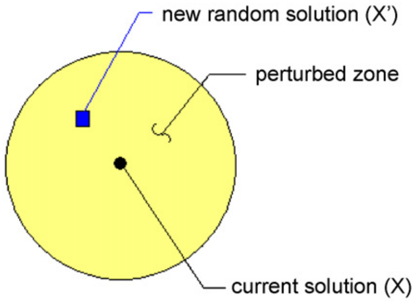

Fig. 9. New random solution in a perturbed zone.

Table 2
Optimal STLs for a one-chamber cross-flow perforated muffler (pure tone)

Item	SA parameters		Results				
	kk	Iter					
1	0.90	50	Aff_1	Aff_2	D_1	D_2	STL (dB)
			0.6102	0.03653	0.1689	0.1689	38.7
			dh_1 (m)	η_1	dh_2 (m)	η_2	Δp (Pa)
			0.003196	0.04929	0.003196	0.04929	14.69
2	0.93	50	Aff_1	Aff_2	D_1	D_2	STL (dB)
			0.5271	0.2406	0.1169	0.1169	54.9
			dh_1 (m)	η_1	dh_2 (m)	η_2	Δp (Pa)
			0.002106	0.03474	0.002106	0.03474	15.62
3	0.96	50	Aff_1	Aff_2	D_1	D_2	STL (dB)
			0.5168	0.2252	0.1105	0.1105	56.9
			dh_1 (m)	η_1	dh_2 (m)	η_2	Δp (Pa)
			0.001971	0.03294	0.001971	0.03294	18.23
4	0.99	50	Aff_1	Aff_2	D_1	D_2	STL (dB)
			0.5501	0.2752	0.1313	0.1313	51.5
			dh_1 (m)	η_1	dh_2 (m)	η_2	Δp (Pa)
			0.002408	0.03878	0.002408	0.03878	11.33
5	<u>0.96</u>	100	Aff_1	Aff_2	D_1	D_2	STL (dB)
			0.5125	0.2188	0.1078	0.1078	57.9
			dh_1 (m)	η_1	dh_2 (m)	η_2	Δp (Pa)
			0.001914	0.03219	0.001914	0.03219	19.49
6	<u>0.96</u>	200	Aff_1	Aff_2	D_1	D_2	STL (dB)
			0.5125	0.2188	0.1078	0.1078	57.9
			dh_1 (m)	η_1	dh_2 (m)	η_2	Δp (Pa)
			0.001914	0.03219	0.001914	0.03219	19.49
7	<u>**0.96**</u>	<u>**2000**</u>	Aff_1	Aff_2	D_1	D_2	STL (dB)
			<u>**0.5001**</u>	<u>**0.2001**</u>	<u>**0.1000**</u>	<u>**0.1000**</u>	<u>**61.0**</u>
			dh_1 (m)	η_1	dh_2 (m)	η_2	Δp (Pa)
			<u>**0.001751**</u>	<u>**0.03001**</u>	<u>**0.001751**</u>	<u>**0.03001**</u>	<u>23.86</u>

Underlined: selected parameter.
Underlined and bold: selected parameter and final results.

$$\Delta F = \mathrm{OBJ}(X') - \mathrm{OBJ}(X), \tag{31b}$$

wherein the C and T are the Boltzmann constant and the current temperature, respectively. Moreover, compared with the new random probability of rand (0, 1), if the transition property (pb(X')) is greater than a random number of rand (0, 1), the new worse solution which results in a higher energy (uphill moves)

Table 3
Optimal STLs for a two-chamber cross-flow perforated muffler (pure tone)

Item	SA parameters		Results					
	kk	Iter						
1	0.90	50	Aff_1	Aff_2	Aff_3	Aff_4	D_1	STL (dB)
			0.3829	0.38290	0.66570	0.6657	0.2829	122.4
			D_2 (m)	D_3 (m)	η_1	dh_1 (m)	η_2	Δp (Pa)
			0.2829	0.2829	0.005590	0.08120	0.005590	11.25
			dh_2 (m)	η_3	dh_3 (m)	η_4	dh_4 (m)	
			0.08120	0.005590	0.08120	0.005590	0.08120	
2	0.93	50	Aff_1	Aff_2	Aff_3	Aff_4	D_1	STL (dB)
			0.3855	0.38550	0.67100	0.6710	0.2855	129.0
			D_2 (m)	D_3 (m)	η_1	dh_1 (m)	η_2	Δp (Pa)
			0.2855	0.2855	0.005645	0.08193	0.005645	8.07
			dh_2 (m)	η_3	dh_3 (m)	η_4	dh_4 (m)	
			0.08193	0.08193	0.005645	0.005645	0.08193	
3	0.96	50	Aff_1	Aff_2	Aff_3	Aff_4	D_1	STL (dB)
			0.3923	0.3923	0.6846	0.6846	0.2923	153.4
			D_2 (m)	D_3 (m)	η_1	dh_1 (m)	η_2	Δp (Pa)
			0.2923	0.2923	0.005788	0.08384	0.005788	10.50
			dh_2 (m)	η_3	dh_3 (m)	η_4	dh_4 (m)	
			0.08384	0.005788	0.08384	0.005788	0.08384	
4	0.99	100	Aff_1	Aff_2	Aff_3	Aff_4	D_1	STL (dB)
			0.3989	**0.3989**	**0.6978**	**0.6978**	**0.2989**	**180.8**
			D_2 (m)	D_3 (m)	η_1	dh_1 (m)	η_2	Δp (Pa)
			0.2989	**0.2989**	**0.005926**	**0.08569**	**0.005926**	10.01
			dh_2 (m)	η_3	dh_3 (m)	η_4	dh_4 (m)	
			0.08569	**0.005926**	**0.08569**	**0.005926**	**0.08569**	

Underlined: selected parameter.
Underlined and bold: selected parameter and final results.

condition will then be accepted. Otherwise, it will be abandoned. Nevertheless, the uphill at a higher temperature has a better chance of escaping from the local optimum. The algorithm will repeat the perturbation of the current solution and the measurement of the change in the objective function. As indicated in Fig. 8, each successful substitution of the new current solution will lead to the decay of the current temperature as

$$T_{\text{new}} = \text{kk}\, T_{\text{old}}, \tag{32}$$

where kk is the cooling rate. Moreover, to reach an initial transition probability $\text{pb}(-\Delta F/CT)$ of 0.5, which will allow uphill moves at a certain ΔF level, the related initial temperature (T_0) is selected as 0.2 [16]. The process is repeated until the predetermined number ($\text{iter}_{\max}$) of the outer loop is reached.

6. Results and discussion

6.1. Results

As described in the above section, slow cooling is more efficient at maintaining a minimal energy state. Therefore, slow cooling (kk) with a range of 0.90–0.99, which was used in the previous work [17], is selected. To investigate the influences of the cooling rate and the number of iterations, the ranges of the SA parameters of the cooling rate and the iterations are:

$$\text{kk} = (0.90, 0.93, 0.96, 0.99), \quad \text{Iter}_{\max} = (50-2000).$$

Table 4
Optimal STLs for a three-chamber cross-flow perforated muffler (pure tone)

Item	SA parameters		Results					
	kk	Iter						
1	0.90	50	Aff_1	Aff_2	Aff_3	Aff_4	Aff_5	STL (dB)
			0.21540	0.2154	0.2154	0.2926	0.2926	100.3
			Aff_6	D_1	D_2 (m)	D_3 (m)	D_4 (m)	Δp (Pa)
			0.2926	0.1386	0.1386	0.1386	0.1386	59.32
			dh_1 (m)	η_1	dh_2 (m)	η_2	dh_3 (m)	
			0.002560	0.04080	0.002560	0.04080	0.002560	
			η_3	dh_4 (m)	η_4	dh_5 (m)	η_5	
			0.04080	0.002560	0.04080	0.002560	0.04080	
			dh_6 (m)	η_6				
			0.002560	0.04080				
2	0.93	50	Aff_1	Aff_2	Aff_3	Aff_4	Aff_5	STL (dB)
			0.2819	0.2819	0.2819	0.6913	0.6913	139.8
			Aff_6	D_1	D_2 (m)	D_3 (m)	D_4 (m)	Δp (Pa)
			0.6913	0.3047	0.3047	0.3047	0.3047	8.04
			dh_1 (m)	η_1	dh_2 (m)	η_2	dh_3 (m)	
			0.006049	0.08732	0.006049	0.08732	0.006049	
			η_3	dh_4 (m)	η_4	dh_5 (m)	η_5	
			0.08732	0.006049	0.08732	0.006049	0.08732	
			dh_6 (m)	η_6				
			0.006049	0.08732				
3	0.96	50	Aff_1	Aff_2	Aff_3	Aff_4	Aff_5	STL (dB)
			0.2962	0.2962	0.2962	0.7774	0.7774	199.1
			Aff_6	D_1	D_2 (m)	D_3 (m)	D_4 (m)	Δp (Pa)
			0.7774	0.3406	0.3406	0.3406	0.3406	5.83
			dh_1 (m)	η_1	dh_2 (m)	η_2	dh_3 (m)	
			0.006802	0.09736	0.006802	0.09736	0.006802	
			η_3	dh_4 (m)	η_4	dh_5 (m)	η_5	
			0.09736	0.006802	0.09736	0.006802	0.09736	
			dh_6 (m)	η_6				
			0.006802	0.09736				
4	0.99	50	Aff_1	Aff_2	Aff_3	Aff_4	Aff_5	STL (dB)
			0.2891	0.2891	0.2891	0.7348	0.7348	205.0
			Aff_6	D_1	D_2 (m)	D_3 (m)	D_4 (m)	Δp (Pa)
			0.7348	0.3228	0.3228	0.3228	0.3228	6.82
			dh_1 (m)	η_1	dh_2 (m)	η_2	dh_3 (m)	
			0.006429	0.09239	0.006429	0.09239	0.006429	
			η_3	dh_4 (m)	η_4	dh_5 (m)	η_5	
			0.09239	0.006429	0.09239	0.006429	0.09239	
			dh_6 (m)	η_6				
			0.006429	0.0923				
5	0.96	100	Aff_1	Aff_2	Aff_3	Aff_4	Aff_5	STL (dB)
			0.2908	0.2908	0.2908	0.7447	0.7447	217.5
			Aff_6	D_1	D_2 (m)	D_3 (m)	D_4 (m)	Δp (Pa)
			0.7447	0.3270	0.3270	0.3270	0.3270	6.56
			dh_1 (m)	η_1	dh_2 (m)	η_2	dh_3 (m)	
			0.006516	0.006516	0.09355	0.09355	0.006516	
			η_3	dh_4 (m)	η_4	dh_5 (m)	η_5	
			0.09355	0.006516	0.09355	0.006516	0.09355	
			dh_6 (m)	η_6				
			0.006516	0.09355				
6	**0.96**	**200**	Aff_1	Aff_2	Aff_3	Aff_4	Aff_5	STL (dB)
			0.2905	**0.2905**	**0.2905**	**0.7429**	**0.7429**	**218.8**

Table 4 (*continued*)

Item	SA parameters		Results					
	kk	Iter						
			Aff_6	D_1	D_2 (m)	D_3 (m)	D_4 (m)	Δp (Pa)
			0.7429	**0.3262**	**0.3262**	**0.3262**	**0.3262**	6.61
			dh_1 (m)	η_1	dh_2 (m)	η_2	dh_3 (m)	
			0.006501	**0.09334**	**0.006501**	**0.09334**	**0.006501**	
			η_3	dh_4 (m)	η_4	dh_5 (m)	η_5	
			0.09334	**0.006501**	**0.09334**	**0.006501**	**0.09334**	
			dh_6 (m)	η_6				
			0.006501	**0.09334**				

Underlined: selected parameter.
Underlined and bold: selected parameter and final results.

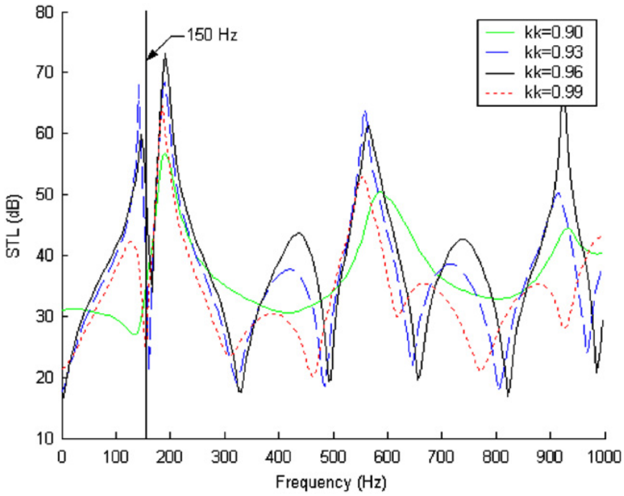

Fig. 10. STL curves with respect to frequencies at various cooling rates for a one-chamber muffler ($iter_{max} = 50$, targeted tone = 150 Hz).

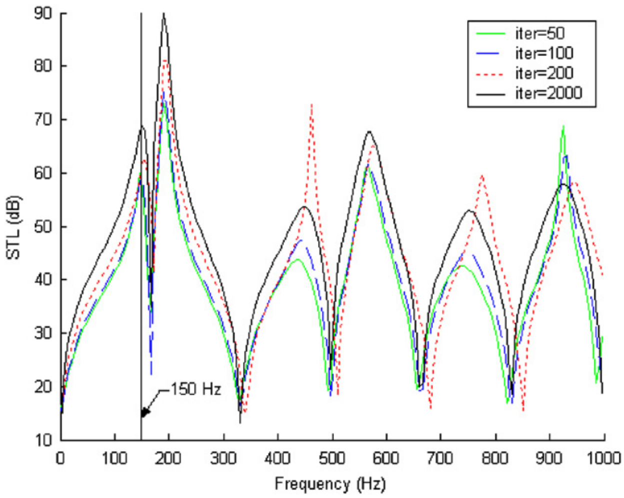

Fig. 11. STL curves with respect to frequencies at various iterations for a one-chamber muffler (kk = 0.96, targeted tone = 150 Hz).

The optimal results with respect to one-tone, two-tone, and broadband noise optimizations are described as follows.

6.1.1. One-tone noise optimization

The maximization of STL with respect to a one-, two-, and three-chamber cross-flow perforated muffler at 150 Hz was performed. As indicated in Tables 2–4, seven set, four set, and six set parameters with respect to three kinds of muffle are tried. Obviously, the optimal design data can be obtained at the last set of SA parameters at (kk, Iter) = (0.96, 2000), (0.99, 100), and (0.96, 200), respectively. Moreover, the pressure drops—Δp (back pressure)—with respect to three kinds of mufflers are found to be 11.33–23.87 (Pa), 8.07–11.25 (Pa), and 5.83–59.32 (Pa). These drops will meet the specified maximal pressure drop of 100 (Pa).

For a one-chamber muffler, the related STLs with respect to various cooling rates (kk) and iterations (Iter) are plotted and illustrated in Figs. 10 and 11, respectively. Likewise, for a two-chamber muffler, the related STLs with respect to different parameters are plotted and illustrated in Fig. 12. Consequently, for a

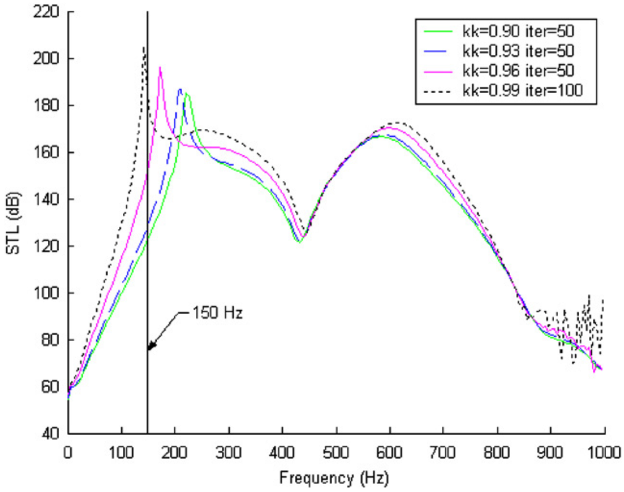

Fig. 12. STL curves with respect to frequencies at various cooling rates and iterations for a two-chamber muffler (targeted tone = 150 Hz).

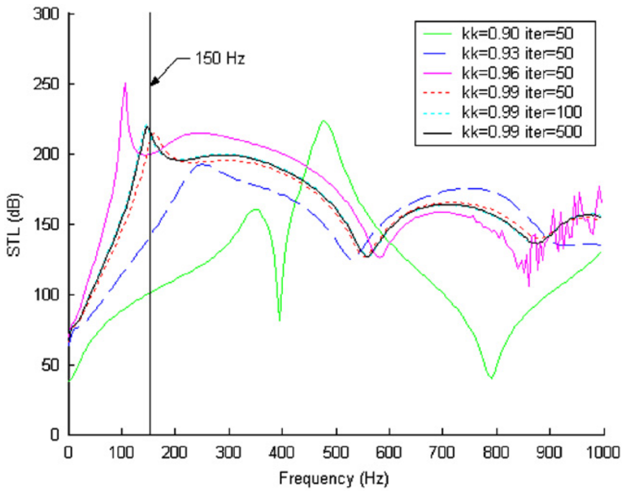

Fig. 13. STL curves with respect to frequencies at various cooling rates and iterations for a three-chamber muffler (targeted tone = 150 Hz).

three-chamber muffler, the related STLs with respect to different parameters are plotted and illustrated in Fig. 13. In addition, the spectrum of the STL curves with respect to these mufflers are plotted together in Fig. 14 simultaneously.

As indicated in Figs. 10–13, the better cooling rate (kk) will occur within 0.96–0.99; moreover, the accuracy of the OBJ value will be significantly improved when the iteration increases. As illustrated in Fig. 14, the more chambers we have in a muffler the better the acoustical performance. Consequently, it is obvious that the maximal STLs with respect to three kinds of mufflers are precisely tuned at the targeted tone of 150 Hz.

6.1.2. Two-tone noise optimization

The maximization of averaged STLs with respect to a one-, two-, and three-chamber cross-flow perforated muffler at 100 and 200 Hz was performed. By using the optimal kk and iteration obtained in pure tone

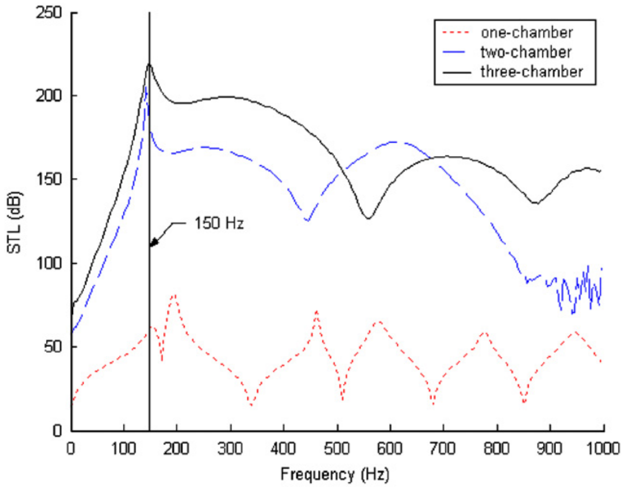

Fig. 14. STL curves with respect to frequencies for three kinds of mufflers (targeted pure tone of 150 Hz).

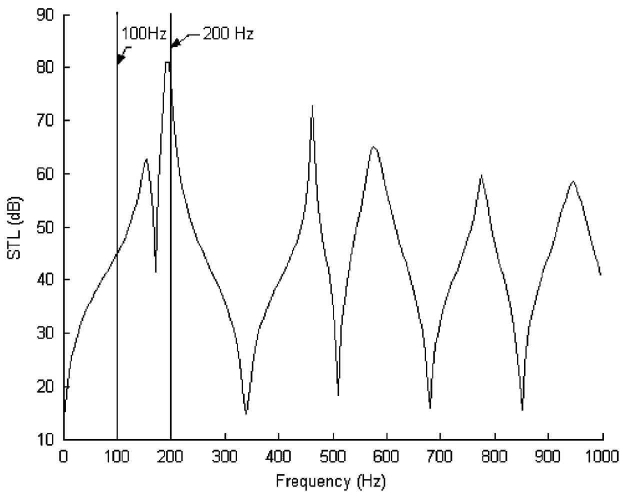

Fig. 15. STL curve with respect to frequencies for a one-chamber muffler (two targeted tones of 100 and 200 Hz). (kk = 0.96; iter = 2000; $\mathrm{Aff}_1 = 0.5001\mathrm{E}+00$; $\mathrm{Aff}_2 = 0.2001\mathrm{E}+00$; $D_1 = 0.1000\mathrm{E}+00$; $D_2 = 0.1000\mathrm{E}+00$; $\mathrm{dh}_1 = 0.1751\mathrm{E}{-}02$; $\eta_1 = 0.3001\mathrm{E}{-}01$; $\mathrm{dh}_2 = 0.1751\mathrm{E}{-}02$; $\eta_2 = 0.3001\mathrm{E}{-}01$; $(\mathrm{STL1}+\mathrm{STL2})/2 = 0.7114\mathrm{E}+02$).

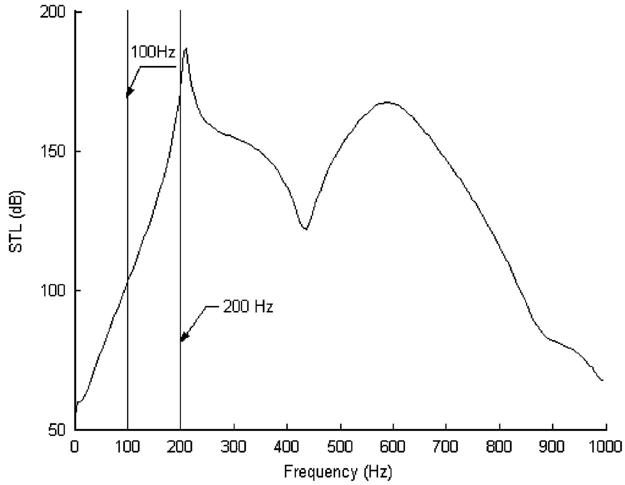

Fig. 16. STL curve with respect to frequencies for a two-chamber muffler (two targeted tones of 100 and 200 Hz) (kk = 0.99; iter = 100; $Aff_1 =$; $Aff_2 = 0.3855E+00$; $Aff_3 = Aff_4 = 6710E+00$; $D_1 = D_2 = D_3 = 0.2855E+00$; $\eta_1 = 0.5645E{-}02$; $dh_1 = 0.8193E{-}01$; $\eta_2 = 0.5645E{-}02$; $dh_2 = 0.8193E{-}01$; $\eta_3 = 0.5645E{-}02$; $dh_3 = 0.8193E{-}01$; $\eta_4 = 0.5645E{-}02$; $dh_4 = 0.8193E{-}01$; $(STL1+STL2)/2 = 0.1383E+03$).

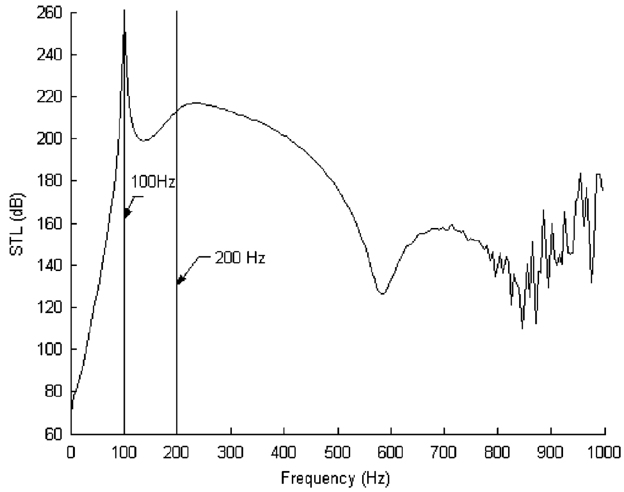

Fig. 17. STL curve with respect to frequencies for a three-chamber muffler (two targeted tones of 100 and 200 Hz) (kk = 0.99, iter = 100, $Aff_1 = 0.2971E+00$, $Aff_2 = 0.2971E+00$, $Aff_3 = 0.2971E+00$, $Aff_4 = 0.7824E+00$, $Aff_5 = 0.7824E+00$, $Aff_6 = 0.7824E+00$, $D_1 = 0.3427E+00$, $D_2 = 0.3427E+00$, $D_3 = 0.3427E+00$, $D_4 = 0.3427E+00$, $dh_1 = 0.6846E{-}02$, $\eta_1 = 0.9794E{-}01$, $dh_2 = 0.6846E{-}02$, $\eta_2 = 0.9794E{-}01$, $dh_3 = 0.6846E{-}02$, $\eta_3 = 0.9794E{-}01$, $dh_4 = 0.6846E{-}02$, $\eta_4 = 0.9794E{-}01$, $dh_5 = 0.6846E{-}02$, $\eta_5 = 0.9794E{-}01$, $dh_6 = 0.6846E{-}02$, $\eta_6 = 0.9794E{-}01$, $(STL1+STL2)/2 = 0.2407E+03$).

analysis, the resultant STL curves of three kinds of mufflers are obtained and shown in Figs. 15–17, respectively. In addition, the spectrum of the STL curves with respect to these mufflers is plotted together in Fig. 18 simultaneously.

6.1.3. Full-band noise optimization

Three kinds of optimal muffler design parameters and sizes in minimizing the fan's sound power level are achieved and summarized in Tables 5–7. As revealed in Tables 5–7, the optimal design data with respect to one-, two-, and three-chamber mufflers occurred in the sixth, fifth, and seventh set, respectively. The related silenced SWLs with respect to three silencers (i.e. one-, two-, and three-chamber muffler) are 96.5, 60.1 and

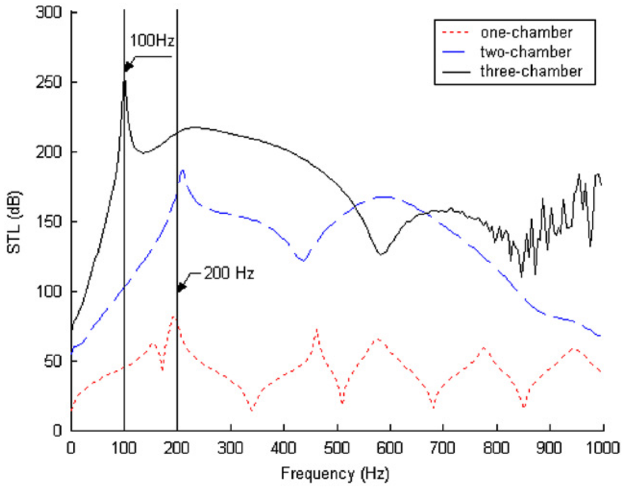

Fig. 18. STL curves with respect to frequencies for three kinds of mufflers (targeted two tones of 100 and 200 Hz).

Table 5
Optimal STLs for a one-chamber cross-flow perforated muffler (broadband)

Item	SA parameters		Results				
	kk	Iter					
1	0.90	50	Aff_1	Aff_2	D_1	D_2	SWL (dB)
			0.7968	0.6452	0.2855	0.2855	110.2
			dh_1 (m)	η_1	dh_2 (m)	η_2	Δp (Pa)
			0.005645	0.08193	0.005645	0.08193	1.31
2	0.93	50	Aff_1	Aff_2	D_1	D_2	SWL (dB)
			0.8329	0.6993	0.3080	0.3080	104.9
			dh_1 (m)	η_1	dh_2 (m)	η_2	Δp (Pa)
			0.006119	0.08825	0.006119	0.08825	1.08
3	0.96	50	Aff_1	Aff_2	D_1	D_2	SWL (dB)
			0.6102	0.3653	0.1689	0.1689	103.8
			dh_1 (m)	η_1	dh_2 (m)	η_2	Δp (Pa)
			0.003196	0.0929	0.003196	0.04929	5.60
4	0.99	50	Aff_1	Aff_2	D_1	D_2	SWL (dB)
			0.5501	0.2752	0.1313	0.1313	99.6
			dh_1 (m)	η_1	dh_2 (m)	η_2	Δp (Pa)
			0.002408	0.03878	0.002408	0.03878	11.33
5	0.99	100	Aff_1	Aff_2	D_1	D_2	SWL (dB)
			0.5636	0.2954	0.1398	0.1398	96.6
			dh_1 (m)	η_1	dh_2 (m)	η_2	Δp (Pa)
			0.002585	0.04113	0.002585	0.04113	9.53
6	**0.99**	**200**	Aff_1	Aff_2	D_1	D_2	SWL (dB)
			0.5467	**0.2701**	**0.1292**	**0.1292**	**96.5**
			dh_1 (m)	η_1	dh_2 (m)	η_2	Δp (Pa)
			0.002363	**0.03817**	**0.002363**	**0.03817**	11.86

Underlined: selected parameter.
Underlined and bold: selected parameter and final results.

20.3 dB, individually. Moreover, their pressure drops—Δp (back pressure)—with respect to three kinds of mufflers are found to be 1.08–11.86 (Pa), 12.83–59.79 (Pa), and 9.66–87.36 (Pa). They will meet the specified maximal pressure drop of 100 (Pa).

Table 6
Optimal STLs for a two-chamber cross-flow perforated muffler (broadband)

Item	SA parameters		Results					
	kk	Iter						
1	0.90	50	Aff_1	Aff_2	Aff_3	Aff_4	D_1	SWL (dB)
			0.2256	0.2256	0.3512	0.3512	0.1256	73.8
			D_2 (m)	D_3 (m)	η_1	dh_1 (m)	η_2	Δp (Pa)
			0.1256	0.1256	0.002287	0.03716	0.002287	59.79
			dh_2 (m)	η_3	dh_3 (m)	η_4	dh_4 (m)	
			0.03716	0.002287	0.03716	0.002287	0.03716	
2	0.93	50	Aff_1	Aff_2	Aff_3	Aff_4	D_1	SWL (dB)
			0.3518	0.3518	0.6036	0.6036	0.2518	67.5
			D_2 (m)	D_3 (m)	η_1	dh_1 (m)	η_2	Δp (Pa)
			0.2518	0.2518	0.004938	0.07251	0.004938	14.36
			dh_2 (m)	η_3	dh_3 (m)	η_4	dh_4 (m)	
			0.07251	0.004938	0.07251	0.004938	0.07251	
3	0.96	50	Aff_1	Aff_2	Aff_3	Aff_4	D_1	SWL (dB)
			0.3405	0.3405	0.5809	0.5809	0.2405	75.3
			D_2 (m)	D_3 (m)	η_1	dh_1 (m)	η_2	Δp (Pa)
			0.2405	0.2405	0.004700	0.06933	0.004700	15.80
			dh_2 (m)	η_3	dh_3 (m)	η_4	dh_4 (m)	
			0.06933	0.004700	0.06933	0.004700	0.06933	
4	0.99	50	Aff_1	Aff_2	Aff_3	Aff_4	D_1	SWL (dB)
			0.2256	0.2256	0.3512	0.3512	0.1256	73.8
			D_2 (m)	D_3 (m)	η_1	dh_1 (m)	η_2	Δp (Pa)
			0.1256	0.1256	0.002287	0.03716	0.002287	59.79
			dh_2 (m)	η_3	dh_3 (m)	η_4	dh_4 (m)	
			0.03716	0.002287	0.03716	0.002287	0.03716	
5	**0.99**	**100**	Aff_1	Aff_2	Aff_3	Aff_4	D_1	SWL (dB)
			0.3657	**0.3657**	**0.6315**	**0.6315**	**0.2657**	**60.1**
			D_2 (m)	D_3 (m)	η_1	dh_1 (m)	η_2	Δp (Pa)
			0.2657	**0.2657**	**0.005231**	**0.07641**	**0.005231**	12.83
			dh_2 (m)	η_3	dh_3 (m)	η_4	dh_4 (m)	
			0.07641	**0.005231**	**0.07641**	**0.005231**	**0.07641**	

Underlined: selected parameter.
Underlined and bold: selected parameter and final results.

By using the above optimal design data sets obtained from Tables 5–7, the individual theoretical STL curves with three kinds of mufflers are plotted and compared to the SWLO—an un-silenced SWL—in Figs. 19–21. Based on plane wave theory, the proposed theoretical cutoff frequencies of fc_1 ($f_{c1} = (1.84c_o/\pi D)(1 - M^2)^{1/2}$) with respect to three kinds of mufflers (Figs. 19–21) are 652–1555 (Hz), 756–1600 (Hz), and 704–1718 (Hz). Actually, the frequency ranges in Figs. 19–21, which are valid, are below the mentioned cutoff frequencies.

Moreover, the spectrum of the STL curves with respect to the three kinds of mufflers is depicted together in Fig. 22.

6.2. Discussion

For the pure tone's optimization discussed in Section 6.1 and shown in Fig. 14, the maximal STLs with respect to the three kinds of mufflers have been precisely tuned at the targeted pure tone of 150 Hz. Similarly, for a duel tone's optimization depicted in Fig. 18, concerning the weighted factors for two tones that are equal to 0.5, the averaged STLs of the two tones are maximized uniformly. As a result of above observation, the SA method is reliably used in the muffler's shape optimization.

Table 7
Optimal STLs for a three-chamber cross-flow perforated muffler (broadband)

Item	SA parameters		Results					
	kk	Iter						
1	0.90	50	Aff$_1$	Aff$_2$	Aff$_3$	Aff$_4$	Aff$_5$	SWL (dB)
			0.2731	0.2731	0.2731	0.6388	0.6388	40.4
			Aff$_6$	D_1	D_2 (m)	D_3 (m)	D_4 (m)	Δp (Pa)
			0.6388	0.2828	0.2828	0.2828	0.2828	9.92
			dh$_1$ (m)	η_1	dh$_2$ (m)	η_2	dh$_3$ (m)	
			0.005590	0.08120	0.005590	0.08120	0.005590	
			η_3	dh$_4$ (m)	η_4	dh$_5$ (m)	η_5	
			0.08120	0.005590	0.08120	0.005590	0.08120	
			dh$_6$ (m)	η_6				
			0.005590	0.08120				
2	0.93	50	Aff$_1$	Aff$_2$	Aff$_3$	Aff$_4$	Aff$_5$	SWL (dB)
			0.2117	0.2117	0.2117	0.2701	0.2701	46.9
			Aff$_6$	D_1	D_2 (m)	D_3 (m)	D_4 (m)	Δp (Pa)
			0.2701	0.1292	0.1292	0.1292	0.1292	69.67
			dh$_1$ (m)	η_1	dh$_2$ (m)	η_2	dh$_3$ (m)	
			0.002363	0.03817	0.002363	0.03817	0.002363	
			η_3	dh$_4$ (m)	η_4	dh$_5$ (m)	η_5	
			0.03817	0.002363	0.03817	0.002363	0.03817	
			dh$_6$ (m)	η_6				
			0.002363	0.03817				
3	0.96	50	Aff$_1$	Aff$_2$	Aff$_3$	Aff$_4$	Aff$_5$	SWL (dB)
			0.2117	0.2117	0.2117	0.2701	0.2701	29.9
			Aff$_6$	D_1	D_2 (m)	D_3 (m)	D_4 (m)	Δp (Pa)
			0.2701	0.1292	0.1292	0.1292	0.1292	69.67
			dh$_1$ (m)	η_1	dh$_2$ (m)	η_2	dh$_3$ (m)	
			0.002363	0.03817	0.002363	0.03817	0.002363	
			η_3	dh$_4$ (m)	η_4	dh$_5$ (m)	η_5	
			0.03817	0.002363	0.03817	0.002363	0.03817	
			dh$_6$ (m)	η_6				
			0.002363	0.03817				
4	$\underline{0.99}$	50	Aff$_1$	Aff$_2$	Aff$_3$	Aff$_4$	Aff$_5$	SWL (dB)
			0.2742	0.2742	0.2742	0.6452	0.6452	37.7
			Aff$_6$	D_1	D_2 (m)	D_3 (m)	D_4 (m)	Δp (Pa)
			0.6452	0.2855	0.2855	0.2855	0.2855	9.66
			dh$_1$ (m)	η_1	dh$_2$ (m)	η_2	dh$_3$ (m)	
			0.005645	0.08193	0.005645	0.08193	0.005645	
			η_3	dh$_4$ (m)	η_4	dh$_5$ (m)	η_5	
			0.08193	0.005645	0.08193	0.005645	0.08193	

			dh_6 (m)	η_6				
			0.005645	0.08193				
5	0.99	100	Aff_1	Aff_2	Aff_3	Aff_4	Aff_5	SWL (dB)
			0.2169	0.2169	0.2169	0.3012	0.3012	51.0
			Aff_6	D_1	D_2 (m)	D_3 (m)	D_4 (m)	Δp (Pa)
			0.3012	0.1422	0.1422	0.1422	0.1422	55.90
			dh_1 (m)	η_1	dh_2 (m)	η_2	dh_3 (m)	
			0.002636	0.04181	0.002636	0.04181	0.002636	
			η_3	dh_4 (m)	η_4	dh_5 (m)	η_5	
			0.04181	0.002636	0.04181	0.002636	0.04181	
			dh_6 (m)	η_6				
			0.002636	0.04181				
6	0.99	200	Aff_1	Aff_2	Aff_3	Aff_4	Aff_5	SWL (dB)
			0.2075	0.2075	0.2075	0.2451	0.2451	21.7
			Aff_6	D_1	D_2 (m)	D_3 (m)	D_4 (m)	Δp (Pa)
			0.2451	0.1188	0.1188	0.1188	0.1188	84.26
			dh_1 (m)	η_1	dh_2 (m)	η_2	dh_3 (m)	
			0.002144	0.03526	0.002144	0.03526	0.002144	
			η_3	dh_4 (m)	η_4	dh_5 (m)	η_5	
			0.03526	0.002144	0.03526	0.002144	0.03526	
			dh_6 (m)	η_6				
			0.002144	0.03526				
7	**0.96**	**400**	Aff_1	Aff_2	Aff_3	Aff_4	Aff_5	SWL (dB)
			0.2068	**0.2068**	**0.2068**	**0.2406**	**0.2406**	**20.3**
			Aff_6	D_1	D_2 (m)	D_3 (m)	D_4 (m)	Δp (Pa)
			0.2406	**0.1169**	**0.1169**	**0.1169**	**0.1169**	87.36
			dh_1 (m)	η_1	dh_2 (m)	η_2	dh_3 (m)	
			0.002106	**0.03474**	**0.002106**	**0.03474**	**0.002106**	
			η_3	dh_4 (m)	η_4	dh_5 (m)	η_5	
			0.03474	0.002106	0.03474	0.002106	0.03474	
			dh_6 (m)	η_6				
			0.002106	0.03474				

Underlined: selected parameter.
Underlined and bold: selected parameter and final results.

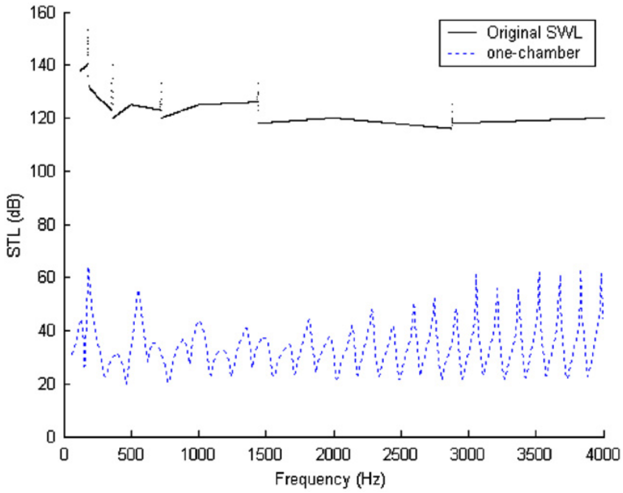

Fig. 19. STL curves and an original SWL with respect to frequencies for a one-chamber muffler (broadband).

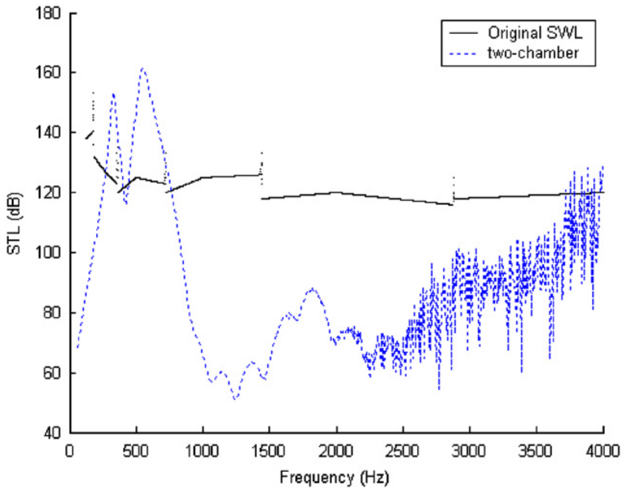

Fig. 20. STL curves and an original SWL with respect to frequencies for a two-chamber muffler (broadband).

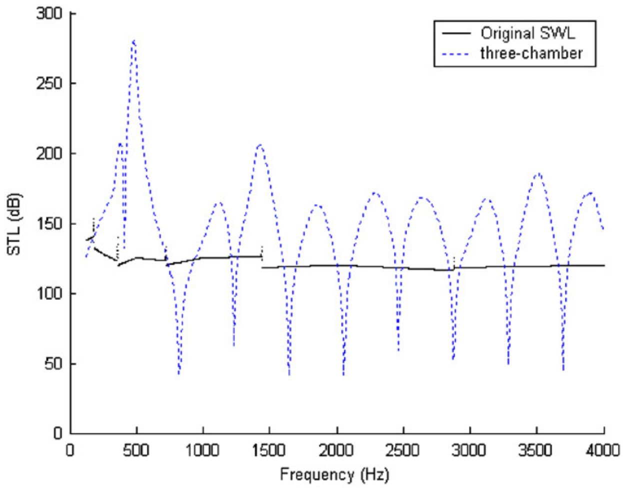

Fig. 21. STL curves and an original SWL with respect to frequencies for a three-chamber muffler (broadband).

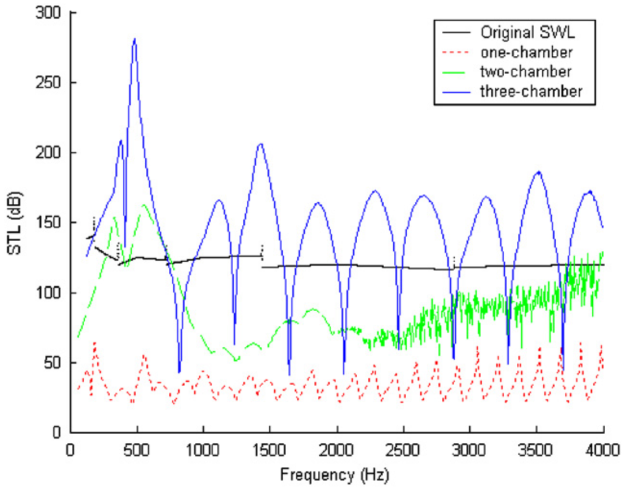

Fig. 22. STL curves and an original SWL with respect to frequencies for three kinds of mufflers (broadband noise).

Table 8
Influence of STLs and Δp with respect to η_i, M_i D_o/D_i and x_i for a one-chamber cross-flow perforated muffler (pure tone of 150 Hz)

Item	Parameters								Targeted OBJ	Back pressure
	η_1	η_2	M_1	M_2	D_o/D_1	D_o/D_2	x_1	x_2	STL (dB)	Δp (Pa)
1	0.049	0.0493	0.0039	0.0039	11.84	11.84	0.0852	0.0852	38.7	14.69
2	0.0347	0.035	0.0081	0.0081	17.10	17.10	0.5720	0.5720	54.9	15.62
3	0.0329	0.033	0.0091	0.0091	18.09	18.09	0.5370	0.5370	56.9	18.23
4	0.0388	0.039	0.0064	0.0064	15.23	15.23	0.6502	0.6502	51.5	11.33
5	0.0322	0.032	0.0095	0.0095	18.55	18.55	0.5226	0.5226	57.9	19.49
6	0.003	0.003	0.0111	0.0111	20	20	0.4804	0.4804	61	23.87

In dealing with a broadband noise in which the spectrum is complicated and emitted from a noisy fan, the selection of the appropriate SA parameters set is indispensable in searching for a better shape design solution within the three kinds of mufflers. As illustrated in Tables 5–7, the optimal design data for three kinds of mufflers has been achieved at (kk, Iter) of (0.99, 200), (0.99, 100), and (0.96, 400), respectively. According to these tables, it is found that the overall noise reduction with respect to three mufflers (one, two, and three chambers) can reach 42.4, 78.8, and 118.6 dB, respectively.

To appreciate the influence of STL and Δp with respect to other parameters such as Mach number (M_i), porosity (η_i), expansion ratio (D_o/D_i), and open area (x_i) for a one-chamber cross-flow muffler, Table 2 is transformed into Table 8. As indicated in Table 8, it is obvious that the STL is proportional to the Mach number (M_i) and expansion ratio (D_o/D_i) and inversely proportional to the porosity (η_i). As shown in Figs. 14, 18, and 22, the muffler with three chambers obviously has the best acoustical performance. Conversely, the single-chamber muffler has the worst. In addition, the pressure drop (i.e. back pressure) of the mufflers is proportional to the Mach number (M_i) and inversely proportional to the porosity (η_i). The above observation of one-chamber cross-flow mufflers is consistent with studies by our experimental data and Munjal et al. [13].

Consequently, the number of chambers, Mach number (M_i), porosity (η_i), and expansion ratio (D_o/D_i) play essential roles in eliminating the noise level in mufflers.

7. Conclusion

It has been shown that two kinds of SA parameters—kk, Iter—play essential roles in seeking a better solution during the SA optimization. A higher iteration will lead to a set of enhanced data. Before broadband noise optimization is performed, the pure-tone and duel-tone optimization of mufflers (one-, two-, and three-chamber mufflers) has been carried out. Results reveal that the maximal STL located around the desired tones is acceptable. To avoid the excessive backpressure occurring in a venting fan, which may lower the venting flow rate, the value of Δp has been calculated and rechecked. As stated in Section 6, several parameters—the number of chambers, Mach number (M_i), porosity (η_i), and expansion ratio (D_o/D_i)—dominate the acoustical performance. Without a doubt, the acoustical mechanism of a cross-flow muffler with three chambers in serial exhibits better noise reduction than that of the mufflers with less acoustical chambers.

Consequently, this study offers a quick and efficient methodology to comprehensively design well-shaped multi-chamber cross-flow mufflers within a confined space. It also satisfies the requirement of the allowable maximal pressure drop for the fan's venting system.

Acknowledgments

The authors acknowledge the financial support of the National Science Council (NSC 95-2218-E-235-002), Taiwan. In addition, the authors would like to thank the reviewers for their help and advice.

References

[1] D.D. Davis, J.M. Stokes, L. Moorse, Theoretical and experimental investigation of mufflers with components on engine muffler design, *NACA Report*, 1954, p. 1192.
[2] M.L. Munjal, K.N. Rao, A.D. Sahasrabudhe, Aeroacoustic analysis of perforated muffler components, *Journal of Sound and Vibration* 114 (2) (1987) 173–188.
[3] J.W. Sullivan, M.J. Crocker, Analysis of concentric tube resonators having unpartitioned cavities, *Acoustical Society of America* 64 (1978) 207–215.
[4] J.W. Sullivan, A method of modeling perforated tube muffler components I: theory, *Acoustical Society of America* 66 (1979) 772–778.
[5] J.W. Sullivan, A method of modeling perforated tube muffler components II: theory, *Acoustical Society of America* 66 (1979) 779–788.
[6] K. Jayaraman, K. Yam, Decoupling approach to modeling perforated tube muffler components, *Acoustical Society of America* 69 (2) (1981) 390–396.
[7] P.T. Thawani, K. Jayaraman, Modeling and applications of straight-through resonators, *Acoustical Society of America* 73 (4) (1983) 1387–1389.
[8] M.L. Munjal, *Acoustics of Ducts and Mufflers with Application to Exhaust and Ventilation System Design*, Wiley, New York, 1987.
[9] K.S. Peat, A numerical decoupling analysis of perforated pipe silencer element, *Journal of Sound and Vibration* 123 (2) (1988) 199–212.
[10] L.J. Yeh, Y.C. Chang, M.C. Chiu, G.J. Lai, GA optimization on multi-segment mufflers under space constraints, *Applied Acoustics* 65 (5) (2004) 521–543.
[11] Y.C. Chang, L.J. Yeh, M.C. Chiu, Shape optimization on double-chamber mufflers using genetic algorithm, *Proceedings of the Institution of Mechanical Engineers Part C: Journal of Mechanical Engineering Science* 10 (2005) 31–42.
[12] L.J. Yeh, Y.C. Chang, M.C. Chiu, Numerical studies on a constrained venting system with reactive mufflers by GA optimization, *International Journal for Numerical Methods in Engineering* 65 (2006) 1165–1185.
[13] M.L. Munjal, K. Krishnan, M.M. Reddy, Flow-acoustic perforated element mufflers with application to design, *Noise Control Engineering Journal* 40 (1) (1993) 159–167.
[14] A. Metropolis, W. Rosenbluth, M.N. Rosenbluth, H. Teller, E. Teller, Equation of static calculations by fast computing machines, *The Journal of Chemical Physics* 21 (6) (1953) 1087–1092.
[15] S. Kirkpatrick, C.D. Gelatt, M.P. Vecchi, Optimization by simulated annealing, *Science* l.220 (4598) (1983) 671–680.
[16] L. Nolle, D.A. Armstrong, A.A. Hopgood, J.A. Ware, Simulated annealing and genetic algorithms applied to finishing mill optimization for hot rolling of wide steel strip, *International of Knowledge-Based Intelligent Engineering System* 6 (2) (2002) 104–111.
[17] Y.C. Chang, L.J. Yeh, M.C. Chiu, Optimization of composite absorbers on constrained sound reverberant system by using simulated annealing, *Applied Acoustics* 66 (2005) 341–352.